Systematic tight-binding study of optical second-harmonic generation in carbon nanotubes

Thomas G. Pedersen and Kjeld Pedersen
Department of Physics and Nanotechnology, Aalborg University, DK-9220 Aalborg Øst, Denmark
(Received 19 November 2008; published 30 January 2009)

Second-harmonic generation spectra for a wide range of carbon nanotubes are computed within a nonorthogonal tight-binding approach. It is demonstrated that a broken $\pi-\pi^*$ symmetry is a prerequisite for a nonvanishing nonlinear response. We study the diameter and chirality dependences of the response and find that optimal values exist for both parameters. Hence, for semiconducting nanotubes the largest response is obtained for diameters around 15 Å. For metallic structures, second-harmonic generation is weak in general.

DOI: 10.1103/PhysRevB.79.035422 PACS number(s): 78.67.Ch, 42.70.−a

I. INTRODUCTION

Efficient optical harmonic generation in carbon nanotubes (CNs) has been predicted theoretically for the cases of second-harmonic generation (SHG),[1,2] third-harmonic generation,[3–5] as well as high-harmonic generation.[6,7] Several of these theoretical results have been verified experimentally.[4,8–10] In particular, Su *et al.*[10] reported spectroscopic SHG measurements for 4 Å CNs. A pronounced resonance attributed to (4,2) CNs was found to dominate the response in agreement with the pioneering calculations of Guo *et al.*[1] Hence, there are strong indications that efficient resonant harmonic generation opens a window to different applications as well as fundamental studies of CNs.

The linear optical properties of CNs have been the subject of countless theoretical and experimental investigations. The influence of CN geometry on the free-carrier (independent particle) optical response is rather well understood[11] and complete tables of structure-assigned optical resonances exist.[12] Moreover, excitonic effects have been studied theoretically at both $\vec{k}\cdot\vec{p}$ (Ref. 13) and effective-mass[14] and Bethe-Salpeter equation-based[15–17] levels of sophistication. In comparison, however, the nonlinear optical response is understood only at a rudimentary level. In particular, many questions remain unanswered for even-order effects such as SHG. To obtain a large dipole-allowed response, these effects require broken inversion symmetry, i.e., noncentrosymmetry. This must be considered both for the individual CNs, which must therefore be chiral,[1] but also for collections of CNs since normal samples contain a racemic mixture of left- and right-handed tubes. In this connection, the surprisingly large response of racemic mixtures of chiral CNs reported in Ref. 10 requires an explanation. In analogy with the linear optical response, excitons are expected to modify the nonlinear response significantly. At present, virtually nothing is known about the effect of excitons on location or magnitude of the nonlinear optical resonances. Moreover, nonlinear excitations in CNs are complicated by the possibility of creating biexciton complexes that are expected to be stable even at room temperature.[18] Finally, although a large SHG response has been predicted for small-diameter CNs, it is clear that this cannot hold true for arbitrarily large nanotubes. The reason is that the properties of such large tubes approach those of graphene, which is a centrosymmetric material with vanishing dipole response. Hence, an optimum CN diameter for the SHG response is expected.

Previously, the SHG response has been calculated only for a few small-diameter chiral[1] and deformed achiral[2] CNs using density-functional theory (DFT). For the (4,2) CN, Ref. 1 predicted a resonance around 2 eV, in agreement with experiments,[10] as well as a pronounced shoulder on the low-energy side, which was not observed experimentally. In Ref. 2, only the imaginary part of the nonlinear response is reported but apparently a similar shoulder is predicted. This discrepancy may be an indication that substantial excitonic effects modify the response. Before addressing such issues theoretically, however, a detailed understanding of single-particle effects in the nonlinear response is required. Hence, in the present work, we consider a wide range of diameters and chiralities in order to provide a systematic study of the geometry dependence of SHG in the single-particle approximation. By working within a (nonorthogonal) tight-binding model, we are able to treat very large structures with extremely high numerical accuracy. Specifically, we consider CNs up to the (34,17) structure with as many as 476 atoms in the unit cell. Also, high numerical accuracy is obtained by sampling 500 k points in the Brillouin zone combined with an accurate treatment of singular spectral functions. Our calculations allow us to provide a detailed picture of the (1) diameter dependence and (2) chirality dependence of the nonlinear response. In particular, the limiting behavior as the CN diameter increases and the structure approaches planar graphene is studied. We find that the nonlinear response peaks around a CN diameter of 15 Å. Also, general trends in the nonlinear response are identified and spectral features are interpreted in terms of the band structure. In particular, we demonstrate that $\pi-\pi^*$ asymmetry is essential for a nonvanishing response even in chiral CNs. The present calculations can be regarded as benchmark tight-binding spectra. As such, they provide an excellent reference for studies of excitons in the SHG response. This will be the subject of future work.

II. THEORY AND METHODS

We begin by outlining the approach used to compute the nonlinear optical response. In accordance with Refs. 1 and 2, we focus on the dominating interband response and work within the independent-particle approximation. Also, it is convenient computationally to start from the imaginary part of the response in the limit of vanishing broadening. Subse-

quently, we then add broadening via a convolution with a Gaussian line-shape function and apply the Kramers-Kronig transformation to compute the real part of the response. Therefore, the appropriate second-order response function at pump frequency ω is[19]

$$\mathrm{Im}\,\chi^{(2)}_{xyz}(\omega)=\frac{e^3}{2\hbar^2\omega^3m^3A}\int\sum_{i\in v,j\in c,l}\left[\frac{P_{ijl}}{\frac{1}{2}\omega_{ji}-\omega_{li}}\delta(2\omega-\omega_{ji})+\left\{\frac{P_{ilj}}{\omega_{ji}+\omega_{jl}}+\frac{P_{jli}}{\omega_{ji}+\omega_{li}}\right\}\delta(\omega-\omega_{ji})\right]dk. \quad (1)$$

Here, $\omega_{ji}=\omega_j-\omega_i$ is the transition frequency between states i and j and $P_{ijl}\equiv\mathrm{Im}[p^x_{ij}(p^y_{jl}p^z_{li}+p^z_{jl}p^y_{li})/2]$ with p^α_{ij} as the momentum matrix element along the α direction. We choose the z axis to coincide with the CN long axis. The expression above is identical to the one used in Refs. 1 and 2. However, when written in the present form, the contributions from 2ω resonances ($2\omega\approx\omega_{ji}$) and ω resonances ($\omega\approx\omega_{ji}$) are clearly brought out. The indices in the summation are taken to mean that i and j run over occupied and empty states, respectively, whereas no restrictions are placed on l other than $l\neq i,j$. Finally, we follow Refs. 1 and 2 and choose to normalize with an area $A=\pi[(D/2+d/2)^2-(D/2-d/2)^2]=\pi Dd$, where D and $d=3.35$ Å are the CN diameter and wall thickness, respectively. Such normalization corresponds to omitting the hollow core of the CN from the volume used to obtain the macroscopic response of a dense CN sample. We note that all other nonvanishing tensor elements of the nonlinear response are related to the xyz element above via $\chi^{(2)}_{xyz}=\chi^{(2)}_{xzy}=-\chi^{(2)}_{yxz}=-\chi^{(2)}_{yzx}$.

A nearest-neighbor tight-binding description of π-electron states with a hopping integral of $t=-2.89$ eV (Ref. 20) is applied for the computation of eigenstates. Based on these, momentum matrix elements are obtained in the usual manner.[21,22] As we will demonstrate below, the inclusion of nearest-neighbor wave-function overlap is essential for a correct description of the nonlinear response. Hence, the generalized eigenvalue problem reads as

$$\varepsilon_{2p}c_i+\sum_j tc_j=E\left\{c_i+\sum_j sc_j\right\}, \quad (2)$$

where $s\approx0.1$ is the overlap between neighbor π-electron states and $\varepsilon_{2p}\approx-5$ eV is their on-site energy.[23,24] The summations over j include nearest neighbors to the ith site only. In the absence of overlap and on-site corrections, we obtain the usual eigenvalue problem $\Sigma_j tc_j=E^{(0)}c_i$. By comparison, it follows that the corrections are implemented at virtually no cost, however, as the energy eigenvalue including overlap E is related to the one without overlap $E^{(0)}$ via the simple transformation $E=(E^{(0)}+\varepsilon_{2p})/(1+E^{(0)}s/t)$. Moreover, the eigenvectors are identical. Importantly, this correction breaks the $\pi-\pi^*$ symmetry, which would mean that any valence band is accompanied by a conduction band obtained by a mirror reflection about the Fermi energy. In the presence of overlap, this symmetry no longer exists as is evident from the transformation above. As explained below, the accompanying removal of degenerate transitions is a requirement for a nonvanishing nonlinear response in agreement with results for the Faraday rotation in graphene[23] and CNs.[24]

In order to compute the nonlinear response efficiently and accurately, it is essential that appropriate numerical techniques are applied. Two types of singularities are present in Eq. (1): delta functions and resonant denominators. The method applied to handle singular integrands is exemplified by the last term of Eq. (1) for which we adopt the substitution,

$$\frac{1}{\omega_{ji}+\omega_{jl}}\delta(\omega-\omega_{ji})\rightarrow\frac{\omega_{ji}+\omega_{jl}}{(\omega_{ji}+\omega_{jl})^2+\gamma^2}\delta_w(\omega-\omega_{ji}). \quad (3)$$

Here, the singularity of the resonant denominator is removed by the introduction of a broadening $\hbar\gamma=0.01$ eV. Eventually, all spectra will be convoluted with a line-shape function to simulate the experimentally observed broadening $\hbar\Gamma\sim30$ meV, as explained below. Hence, the magnitude of $\hbar\gamma$ is chosen small enough that the final width is not affected but large enough that numerical instabilities are removed. The delta function is regularized by the adoption of the following discrete approximation:[25]

$$\delta_w(x)=\begin{cases}\frac{1}{w}\left(1-\left|\frac{x}{w}\right|\right), & \left|\frac{x}{w}\right|\leq1\\ 0 & \left|\frac{x}{w}\right|>1.\end{cases} \quad (4)$$

The energy eigenvalues and eigenvectors needed to calculate transition frequencies and matrix elements in Eq. (1) are computed on a regular grid of k points k_n with $n=1,\ldots,n_{\max}$ covering the positive half of the Brillouin zone. Accordingly, the k integral is replaced by a discrete summation over k points. To evaluate the discrete delta function at the mth point, we need the transition frequency $\omega_{ji}(k_m)$ as well as the broadening given by $w=|\omega_{ji}(k_{m+1})-\omega_{ji}(k_{m-1})|$.[25] More sophisticated approximations for the delta function exist[25] but were not found to improve results significantly. To achieve sufficient k-point resolution, it was found that $n_{\max}=500$ was needed. Finally, the response must be evaluated at an extremely fine grid of ω values in order to capture resonances with sufficient accuracy. It was found that as many as 100 000 values in the range 0–5 eV were required for this purpose. As an example, the nonlinear response of a (4,2) nanotube is shown in Fig. 1. The response is clearly dominated by several highly peaked resonances. The shape of these resonances basically reflects the density of states of the one-dimensional (1D) structure $\sim1/\sqrt{\omega-\omega_g}$ above an energy gap $\hbar\omega_g$. Thus, it is mainly the singular nature of the 1D density of states that necessitates such a fine ω sampling.

The resonance structure in Fig. 1 is readily explained from the simplified band diagram in Fig. 2. To highlight the role of the wave-function overlap, it is instructive to consider the simplifying case for which $\pi-\pi^*$ symmetry remains valid. Hence, in Fig. 2, the two lowest conduction and two highest valence bands are positioned symmetrically above and below the Fermi level. Consequently, the c_2-c_1 and v_2-v_1 energy separations are of equal magnitude and denoted as δ in Fig. 2. Also, the fundamental c_1-v_1 band gap is denoted as Δ. Specifically, for the (4,2) nanotube the band

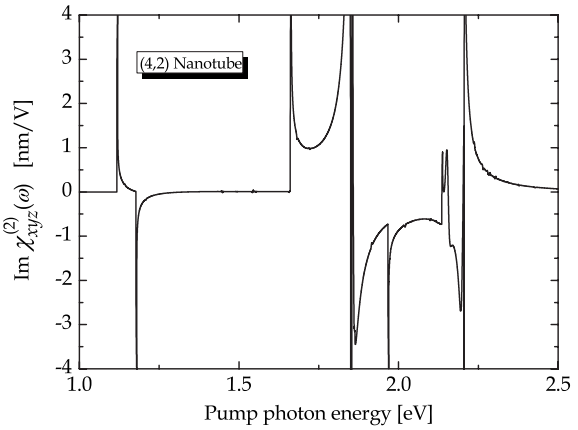

FIG. 1. Imaginary part of the nonlinear response of a (4,2) nanotube.

edges calculated in the simple orthogonal model are located at ± 1.0 and ± 1.75 eV and so one finds $\Delta = 2.0$ and $\delta = 0.75$ eV. The two halves of the figure depict *vvc* processes involving two valence and one conduction band and *vcc* processes involving one valence and two conduction bands, respectively.

The 2ω resonances, i.e., the first term in Eq. (1), are responsible for the low-energy behavior of the response. Hence, naively a 2ω resonance at half the fundamental band gap $\hbar\omega \approx 1$ eV could be expected but, in fact, this transition is forbidden. To see why, it should be noted that the 2ω transitions are between states i and j and, moreover, that the strength of the transition is proportional to p^x_{ij}. The selection rules for CNs are given in, e.g., Refs. 22 and 26. For parallel polarization (z axis), only transitions between symmetrically positioned bands ($v_1 \rightarrow c_1$, $v_2 \rightarrow c_2$, etc.) are allowed; whereas for perpendicular polarization (x and y axes) the allowed transitions are between bands shifted by ± 1 ($v_1 \rightarrow c_2$, $v_2 \rightarrow c_1$, etc.). Consequently, $p^x_{v_1,c_1} = 0$ and the 2ω resonance at $\omega = \Delta/2$ is forbidden. In contrast, $p^x_{v_1,c_2}$, $p^x_{v_2,c_1} \neq 0$, and so a 2ω resonance at $\hbar\omega = (\Delta + \delta)/2$ is expected. Hence, the lowest 2ω resonance coincides with half the band gap

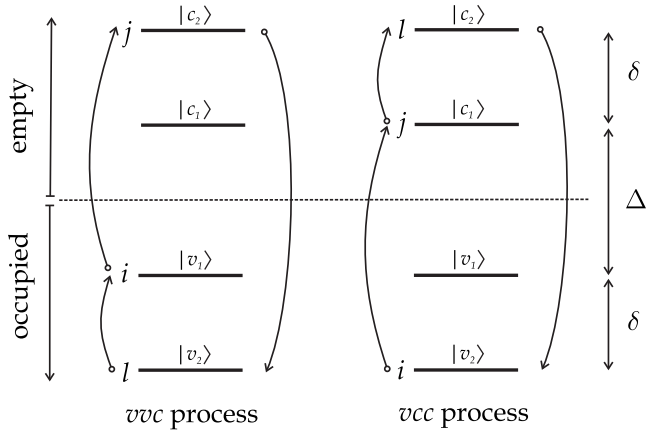

FIG. 2. Schematic level structure assuming $\pi - \pi^*$ symmetry. The transitions responsible for *vvc* and *vcc* processes are indicated in the two panels.

obtained in the linear response for perpendicular polarization. Notice, however, that both *vvc* and *vcc* processes contribute to the nonlinear resonance. As indicated in Fig. 2, the states involved in the two processes are $\{ijl\} = \{v_1 c_2 v_2\}$ and $\{ijl\} = \{v_2 c_1 c_2\}$, respectively. For these two processes, the transition strength P_{ijl} is identical. However, each process is weighted by a factor $(\frac{1}{2}\omega_{ji} - \omega_{li})^{-1}$, [cf. Eq. (1)]. It is readily demonstrated that $\frac{1}{2}\hbar\omega_{ji} - \hbar\omega_{li}$ equals $(\Delta + 3\delta)/2$ and $-(\Delta + 3\delta)/2$ for the *vvc* and *vcc* processes, respectively. Hence, it follows that in the presence of $\pi - \pi^*$ symmetry, the *vvc* and *vcc* processes cancel exactly. When $\pi - \pi^*$ symmetry is lifted by the inclusion of overlap, the four states shift in energy. Hence, for the (4,2) CN the new energy eigenvalues are -6.36, -5.80, -4.15, and -3.46 eV. As a consequence, the *vvc* and *vcc* resonances are now located at $\hbar\omega = 1.17$ and $\hbar\omega = 1.11$ eV, respectively. These transitions are clearly identified in Fig. 1. In addition, the lowest ω resonance coincides with the band gap Δ, which has a magnitude of 1.65 eV after inclusion of overlap. This resonance is also clearly visible in Fig. 1.

III. NONLINEAR SPECTRA

The above theoretical framework has been applied to a wide range of CNs of varying diameter and chirality. For a given (n,m) structure, diameter D and chiral angle α are determined by

$$D = \frac{a}{\pi}\sqrt{n^2 + m^2 + nm}, \quad \alpha = \tan^{-1}\left(\frac{\sqrt{3}m}{2n+m}\right), \tag{5}$$

respectively, where $a = 2.46$ Å is the graphene lattice constant. As $m \leq n$, the chiral angle is restricted to the interval $[0°, 30°]$. The extremal values correspond to zigzag (0°) and armchair (30°) CNs, respectively. Both of these structures are centrosymmetric and yield zero SHG in the dipole limit. Hence, the nonlinear response is expected to peak at some intermediate angle. Similarly, as mentioned above, the diameter dependence is expected to peak at a finite value since large-diameter CNs approach planar (centrosymmetric) graphene and the resonances of small-diameter CNs are pushed up in energy. To quantify these trends, we have investigated the behavior of (a) CNs with varying diameter but fixed chiral angle and (b) CNs with varying chirality but approximately fixed diameter. In case (a), the family of $(2n,n)$ CNs are chosen with n between 2 and 17 covering both semiconductors ($n = 2,4,5,7,\ldots$) and metals ($n = 3,6,9,\ldots$). In case (B), we have studied (8,1), (7,2), (7,3), and (6,4) CNs with diameters between 6.41 and 6.96 Å. The unbroadened imaginary part of the response has been computed using the method described in Sec. II. Subsequently, convolution with the Gaussian $\exp(-\omega^2/\Gamma^2)/\Gamma\sqrt{\pi}$ taking $\hbar\Gamma = 30$ meV is applied. A small broadening (peak width ~ 25 meV) is typically observed in experimental absorption or emission spectra for high-quality samples of dispersed CNs.[27] Thus, the present choice applies to such samples, in which CN bundling is prevented by, e.g., micelle wrapping[27] or zeolite cages.[10] Finally, a numerical Kramers-Kronig transformation provides the real part of the broadened re-

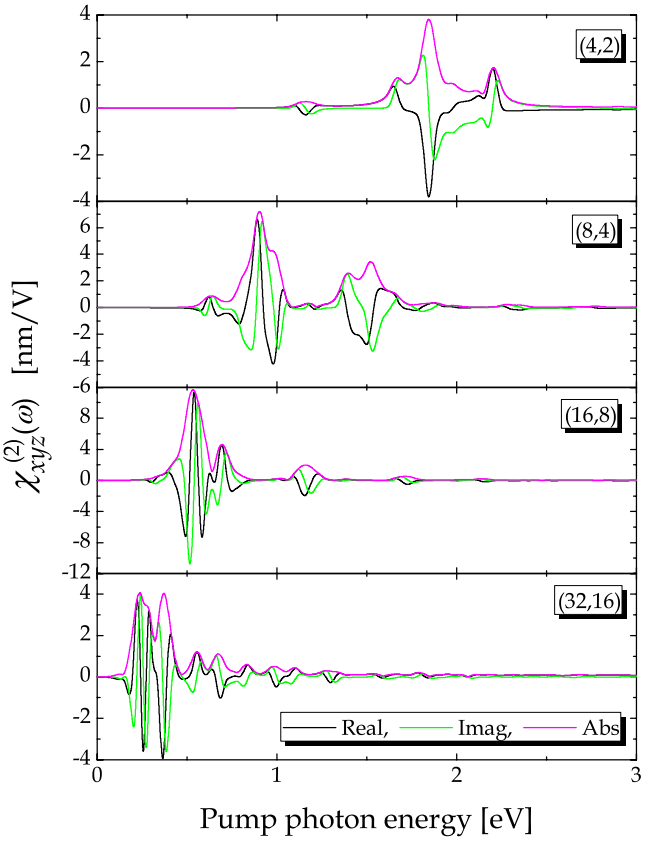

FIG. 3. (Color online) Nonlinear response of four semiconducting members of the $(2n,n)$ family.

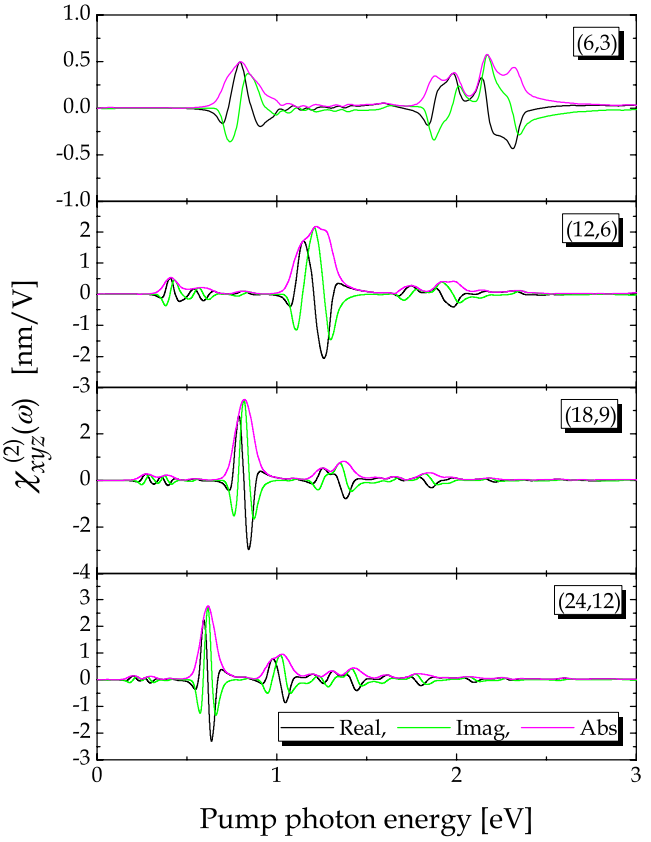

FIG. 4. (Color online) Nonlinear response of four metallic members of the $(2n,n)$ family.

sponse. The real, imaginary, and absolute values of the response for cases [(a) semiconducting], [(a) metallic], and (b) are illustrated in Figs. 3–5, respectively. Eight representative examples of the $(2n,n)$ family are used to illustrate the general trend in case (a).

Several general trends can be extracted from the nonlinear spectra in Figs. 3–5. Focusing first on the diameter dependence in Figs. 3 and 4, it is obvious that all spectral features shift markedly toward lower energy with diameter as expected. It should be noted that high-energy transitions do exist for all geometries but obviously their transition strengths are very low for large-diameter CNs. Hence, the dominant features shift as the inverse diameter following the band gap. Also, comparing semiconducting and metallic CNs, it is clear that the response in the metallic case is significantly less than for semiconductors, especially for smaller diameter CNs. In particular, the low-energy 2ω resonances are suppressed in the metallic structures. To quantify the diameter dependence, we have compared the maximum of the absolute value $|\chi^{(2)}_{xyz}(\omega)|$ in Fig. 6 for all 16 members of the $(2n,n)$ family investigated. This plot very clearly illustrates the observed trend: The response for semiconductors increases roughly linearly with diameter until a maximum around $D=15$ Å is reached. Above this value, a rapid decrease is found. Hence, the (14,7) and (16,8) structures are found to be optimal and, in both cases, the resonance is located close to $\hbar\omega=0.6$ eV. The response of the metallic CNs peaks at a slightly larger diameter and the maximum is roughly 30% of the semiconductor value. However, as the diameter increases, the gap between semiconductors and metals apparently closes. Hence, for very large CNs, both classes of materials will have a similar nonlinear response. Turning finally to the chirality dependence in Fig. 5, we see that the largest response is obtained for the (7,3) structure with a chiral angle of 17° close to the midpoint between the two achiral limits 0° and 30°. For angles either larger or smaller, a reduced response is found but the reduction is more pronounced when the angle is reduced. It is noted that the $(2n,n)$ family has a chiral angle of 19° close to the optimum.

Our results are in reasonable agreement with DFT calculations for the few cases for which DFT-based spectra are available, although the DFT spectra differ somewhat among themselves.[1,2] Hence, converting to esu units (using a conversion factor of 2390 esu V/m), we find a maximum $|\chi^{(2)}_{xyz}(\omega)|$ for the (4,2) CN of 9.6×10^{-6} esu. The corresponding value of Guo *et al.*[1] is approximately 16×10^{-6} esu, although a slightly larger broadening (50 meV) was applied in that study. In contrast, the maximum for the (8,4) structure found in the present work (16.7×10^{-6} esu) is larger than the value reported in Ref. 1 (approximately 10×10^{-6} esu). Thus, simple scaling cannot remove the discrepancies. In general, however, we find that the main spectral features are in qualitative agreement in the two approaches. In particular, for the (4,2) CN, our spectra also display a low-energy shoulder on the main resonance (around 1.8 eV), in clear disagree-

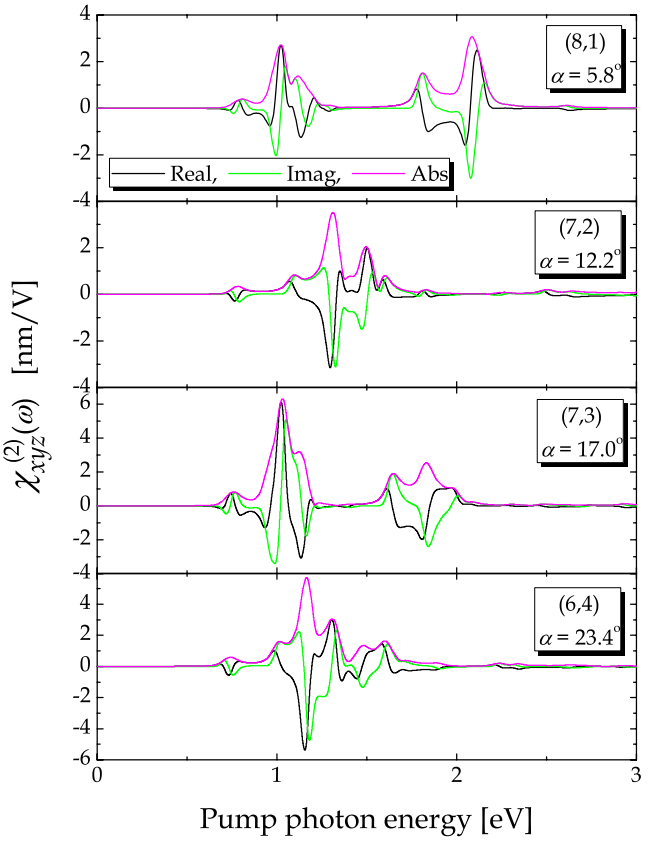

FIG. 5. (Color online) Nonlinear response of four semiconducting CNs with varying chiral angle but similar diameter.

ment with experiments.[10] Hence, the present work suffers from the same problems as DFT-based ones and it is tempting to ascribe the discrepancy to excitons. However, even though excitonic effects are likely to modify the CN response substantially, our results support the conclusion of Refs. 1 and 2 that the nonlinear response at resonance can significantly exceed that of III-V and II-VI inorganic semiconductors typically considered for applications of SHG.

IV. SUMMARY

In summary, a systematic study of second-harmonic generation in small-, medium-, and large-diameter CNs has been

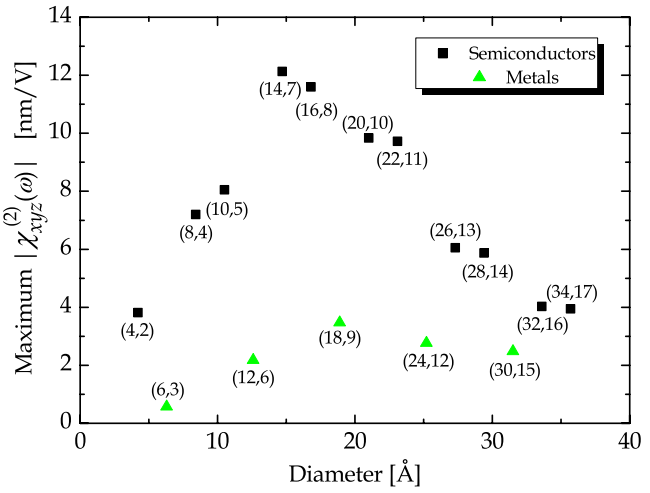

FIG. 6. (Color online) Maximum nonlinear response of semiconducting and metallic members of the $(2n,n)$ family.

presented. Great care has been taken to obtain spectra that are converged with respect to k point and frequency sampling. In addition, the need for a numerically accurate method of treating singularities in the nonlinear response has been pointed out. We have demonstrated that the simplest nearest-neighbor orthogonal tight-binding description of CNs leads to a vanishing nonlinear response because of $\pi-\pi^*$ symmetry. Hence, breaking this symmetry is essential for a correct description and for this purpose wave-function overlap has been included. Within this nonorthogonal model, the location of fundamental spectral features has been given a simple explanation.

We have applied the developed framework to study the diameter and chirality dependences of second-harmonic generation in both semiconductor and metallic CNs. For the $(2n,n)$ family, it is found that the maximum response is obtained around a diameter of 15 Å. Moreover, metallic CNs generally yield a smaller nonlinear response than semiconductors. For a fixed diameter, intermediate chiral angles around $15°-20°$ are found to provide the largest response. The impact of excitons on these conclusions is possibly substantial and will be the subject of future work.

[1] G. Y. Guo, K. C. Chu, D.-S. Wang, and C.-G. Duan, Phys. Rev. B **69**, 205416 (2004).
[2] J. Zhou, H. Weng, G. Wu, and J. Dong, Appl. Phys. Lett. **89**, 013102 (2006).
[3] V. A. Margulis and T. A. Sizikova, Physica B **245**, 173 (1998).
[4] C. Stanciu, R. Ehlich, V. Petrov, O. Steinkellner, J. Herrmann, I. V. Hertel, G. Ya. Slepyan, A. A. Khrutchinski, S. A. Maksimenko, and F. Rotermund, Appl. Phys. Lett. **81**, 4064 (2002).
[5] A. M. Nemilentsau, G. Ya. Slepyan, A. A. Khrutchinskii, and S. A. Maksimenko, Carbon **44**, 2246 (2006).
[6] G. Y. Slepyan, S. A. Maksimenko, V. P. Kalosha, J. Herrmann, E. E. B. Campbell, and I. V. Hertel, Phys. Rev. A **60**, R777 (1999).
[7] O. E. Alon, V. Averbukh, and N. Moiseyev, Phys. Rev. Lett. **85**, 5218 (2000).
[8] S. O. Konorov, D. A. Akimov, A. A. Ivanov, M. V. Alfimov, S. Botti, R. Ciardi, L. De Dominicis, L. S. Asilyan, A. A. Podshivalov, D. A. Sidorov-Biryukov, R. Fantoni, and A. M. Zheltikov, J. Raman Spectrosc. **34**, 1018 (2004).
[9] L. De Dominicis, S. Botti, L. S. Asilyan, R. Ciardi, R. Fantoni, M. L. Terranova, A. Fiori, S. Orlanducci, and R. Appolloni, Appl. Phys. Lett. **85**, 1418 (2004).
[10] H. M. Su, J. T. Ye, Z. K. Tang, and K. S. Wong, Phys. Rev. B **77**, 125428 (2008).
[11] H. Kataura, Y. Kumazawa, Y. Maniwa, I. Umezu, S. Suzuki, Y.

Ohtsuka, and Y. Achiba, Synth. Met. **103**, 2555 (1999).
[12] R. B. Weisman and S. M. Bachilo, Nano Lett. **3**, 1235 (2003).
[13] T. Ando, J. Phys. Soc. Jpn. **66**, 1066 (1997).
[14] T. G. Pedersen, Phys. Rev. B **67**, 073401 (2003).
[15] C. D. Spataru, S. Ismail-Beigi, L. X. Benedict, and S. G. Louie, Phys. Rev. Lett. **92**, 077402 (2004).
[16] V. Perebeinos, J. Tersoff, and Ph. Avouris, Phys. Rev. Lett. **92**, 257402 (2004).
[17] E. Chang, G. Bussi, A. Ruini, and E. Molinari, Phys. Rev. Lett. **92**, 196401 (2004).
[18] T. G. Pedersen, K. Pedersen, H. D. Cornean, and P. Duclos, Nano Lett. **5**, 291 (2005).
[19] E. Ghahramani, D. J. Moss, and J. E. Sipe, Phys. Rev. B **43**, 8990 (1991).
[20] A. Gruneis, R. Saito, Ge. G. Samsonidze, T. Kimura, M. A. Pimenta, A. Jorio, A. G. Souza Filho, G. Dresselhaus, and M. S. Dresselhaus, Phys. Rev. B **67**, 165402 (2003).
[21] T. G. Pedersen, K. Pedersen, and T. B. Kriestensen, Phys. Rev. B **63**, 201101(R) (2001).
[22] A. Zarifi and T. G. Pedersen, Phys. Rev. B **74**, 155434 (2006).
[23] T. G. Pedersen, Phys. Rev. B **68**, 245104 (2003).
[24] A. Zarifi and T. G. Pedersen, Phys. Rev. B **77**, 085409 (2008).
[25] X. Wen, SIAM J. Sci. Comput. (USA) **30**, 1825 (2008).
[26] J. Jiang, R. Saito, A. Grüneis, G. Dresselhaus, and M. S. Dresselhaus, Carbon **42**, 3169 (2004).
[27] M. J. O'Connell, S. M. Bachilo, C. B. Huffman, V. C. Moore, M. S. Strano, E. H. Haroz, K. L. Rialon, P. J. Boul, W. H. Noon, C. Kittrell, J. Ma, R. H. Hauge, R. B. Weisman, and R. E. Smalley, Science **297**, 593 (2002).